Output power improvement of solar pumped single crystal fiber laser based on hollow reflector filled with sensitizing solution

MENGTING SHAO, YAN LIU*, LANLING LAN*, YUANYUAN ZHANG
Center for Astronomy and Space Science, College of Mathematics and Physics, China Three Gorges University, Yichang, Hubei 443002, China

The hollow reflector configuration filled with a fluorescent solution (FITC) as sensitizer is proposed to enhance the output power of solar pumped single crystal fiber (SCF) lasers. A three-stage concentrator comprises parabolic mirror/off-axis parabolic mirrors, 3D-CPC, and a hollow reflector housing the SCF. When the total sunlight-receiving area of the primary concentrator is 1.2 m^2, rays tracing demonstrates that a single- and dual-end-pumped Nd:YAG SCF (Φ1×100 mm, 1 at.% doping concentration) exhibit 21.29% and 17.31% enhancements in absorbed power, respectively, compared to non-sensitized systems. In the single-end-pumped configuration, 104.58 W of solar power is absorbed by the SCF. Numerical calculations indicate that the laser output power is 31.38 W, which is 14.32% higher than that of non-sensitized systems. This provides an idea to further enhance the output power of the SCF lasers pumped by sunlight.

(Received September 8, 2025; accepted December 2, 2025)

Keywords: Solar pumped laser, Parabolic mirror, Single crystal fiber, Fluorescent sensitizer

1. Introduction

With rapid depletion of fossil fuel resources, solar energy has emerged as prominent candidate for sustainable alternative energy solutions [1-2]. The solar pumped lasers (SPLs), representing an advanced approach to solar energy conversion, have received widespread attention owing to great prospects in space laser communication, space solar power stations (SSPS), and magnesium energy cycle, et al. [3-7]. With excellent heat dissipation and high quantum efficiency [8-10], the SCF is considered a promising laser medium for SPLs [11]. Disc and slab also have good heat dissipation, and have been acted as gain medium of solar-pumped lasers [12-13]. In fact, with the advancement of SCF [14-15] and its cladding fabrication technologies [16], SCF lasers and amplifiers can achieve breakthroughs in laser power and efficiency. SCFs with a diameter of approximately 1mm and a length of several hundred millimeters have been fabricated using the laser heated pedestal growth method [17].

Due to the divergence nature and broad emission spectrum of solar radiation, the focus size of primary solar concentrator is large, which leads to lower coupling efficiency and lower output power of fiber laser pumped by sunlight [18]. To improve the conversion efficiency of solar pumped laser, several methods have been employed, including efficient solar concentrator [19], multi-rod configuration [20-21], and sensitizer ion doping [22-23], etc. Due to the small end face of the fiber, the output power of solar end-pumped fiber laser is very low, and the side-pumping is often employed to improve the output power [11]. To enhance the absorbed power of the optical fiber, one approach is that the reflective cavity coiled around the fiber is filled with an appropriate fluorescent sensitization solution, which fluorescence spectrum excited matches the absorption spectrum of the rare-doped fiber. In 2017, T. Masuda et al. reported a solar-pumped fiber laser configuration employing a Nd-doped fiber (~40 m) coiled in the reflective cavity with Rhodamine 6G (R6G). The excitation fluorescence band (~580 nm) generated by R6G matched the Nd-doped fiber's absorption spectrum, and the results demonstrated that R6G could improve the absorption efficiency [24]. A solar side-pumped fiber laser was demonstrated in 2019, and the simulation showed that the output power could be increased from 29 mW to 150 mW when the fiber was dipped into R6G [25]. In 2020, a solar side-pumped Nd-doped fiber configuration with theoretical solar-laser conversion efficiency of 8% was reported based on the R6G [26]. To our knowledge, it is the highest conversion efficiency reported for solar pumped laser. In the same year, this group reported a solar-pumped Nd-doped fiber laser by comparing the performance of a fully inorganic cesium lead halide chalcogenide ($CsPbBr_xI_{3-x}$) with that of R6G as

sensitizers, and calculations indicated that the laser output power obtained with $CsPbBr_xI_{3-x}$ was 2.7 times higher than that achieved with the R6G sensitizer [27]. In 2023, A. A. Sherniyozov et al. reported that a 10.26% increase in output power can be obtained if a 190 m fiber was immersed in a reflective cavity filled with R6G solution without a concentrator [28].

However, the absence of solar concentrators significantly restricts the potential enhancement in output power [24-28], and the excessive fiber length significantly increases the total system expenditure. To enhance the output power of solar-pumped SCF, a cylindrical reflector filled with a sensitization solution is proposed. The parabolic mirror or off-axis parabolic mirrors act as the primary concentrator. Nd:YAG SCFs are selected as gain medium owing to high thermal conductivity and widespread application in laser system [29]. The ray tracing shows that single-end-pumped Nd:YAG SCF (Φ1×100 mm, 1 at. % doping concentration) can improve the absorbed solar power of the SCF by 21.29% compared to non-sensitized systems. The calculated laser output power can be as high as 31.38 W, which is 14.32% higher than that of non-sensitized systems.

2. Concentrator system for single- and dual-end-pumped configurations

In solar concentration systems, transmissive components like Fresnel lenses exhibit pronounced dispersion that results in focal spot enlargement. However, reflective concentrator without dispersion characteristics, such as parabolic mirrors, are increasingly employed as primary solar concentrator. When the total sunlight-receiving area of primary concentrator (parabolic mirror or off-axis parabolic mirrors) and the radius of hollow reflector are 1.2 m^2 and 3 mm, the SCF's absorption characteristics of single- and dual-end-pumped SCF lasers are compared with. The DDE (Dynamic Data Exchange) technology is used to establish an information exchange channel between Matlab and TracePro, which can greatly enhance the design efficiency of solar concentrator for solar pumped laser [19]. DDE technology is particularly important in the process of multi-variable optical design. Therefore, based on DDE technology, a simulated annealing algorithm is used to optimize the parabolic mirror focal length and 3D-CPC inlet radius to achieve that the concentration efficiency of sunlight entering the hollow reflector exceed 90%. A SCF (Φ1 mm × 250 mm, doping concentration of 1 at.%) is placed on the central axis of the hollow-column reflector. The sunlight is reflected many times in the hollow reflector and absorbed by the SCF, and the laser oscillation can be achieved. The absorption characteristics of the SCF can be analyzed by ray tracing based on Tracepro. The solar spectrum is AM1.5, and solar irradiance is set to 1000 W/m^2 by taking into account atmospheric absorption losses [30]. In the rays tracing, the number of rays is 200,000.

The configuration of single-end-pumped SCF laser is indicated in Fig. 1(a). The concentrator system consists of a parabolic reflector (R=620 mm, F_1=1000 mm), a 3D-CPC, and a hollow cylindrical reflector. The SCF is placed in a glass tube, which outer diameter, inner diameter and a length are 0.8 mm, 0.65 mm and 100 mm, respectively. The SCF is cooled by circulating water in the glass tube. The hollow reflector is filled with FITC (Fluorescein Isothiocyanate) fluorescent material, and the inner wall of the reflector has high reflective film (98%) to sunlight. The schematic configuration of the dual-end-pumped SCF laser is demonstrated in Fig. 1(b). Two same off-axis parabolic mirrors (the sunlight-receiving area of each one is 0.6 m^2), two 3D-CPCs and a hollow-column reflector make up the dual-end-pumped concentrator system. The inner and outer radii, the focal length F_2 of the off-axis parabolic mirrors are 1480 mm, 2120 mm and 900 mm, respectively.

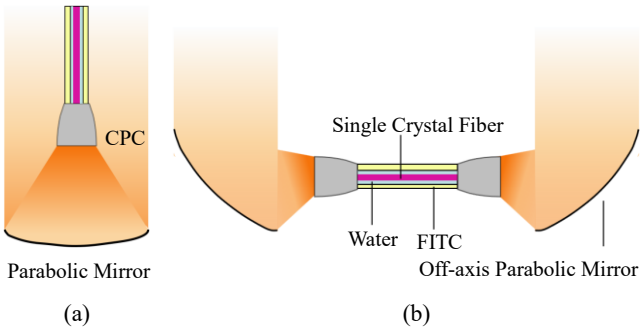

Fig. 1. Schematic configuration of solar single- and dual-end-pumped SCF lasers (colour online)

Firstly, the absorption characteristics of SCF is discussed when the reflector is not filled with fluorescent sensitization solution. The sunlight spirally propagates within the reflector, and the absorbed power of fiber is the least when the fiber offset distance is 0. Therefore the optimal position of fiber is placed at 2 mm offset from the central axis to maximize the absorbed power of the SCF. However, the optimal position of the SCF in dual-end-pumped configuration is at 1.4 mm offset from the central axis. The maximum absorbed power of single-end-pumped and dual-end-pumped SCFs along the length of the SCF is shown in Fig. 2. It is found that the solar power absorbed by dual-end-pumped SCF has always been higher than that of the single-end-pumping. In single- and dual-end-pumped configurations, the concentration efficiency of the sunlight entering the hollow reflector is 91% and 94%, respectively. This reason is that the sunlight-receiving area of one off-axis parabolic mirror is only a half that of parabolic mirror (1.2 m^2), leading to smaller focus and higher concentrating efficiency of sunlight entering into hollow reflector.

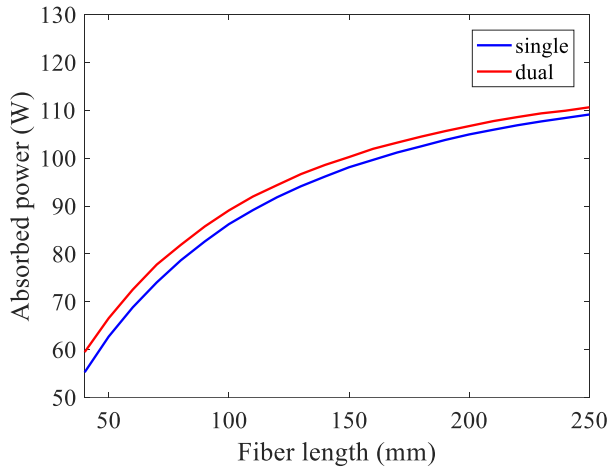

Fig. 2. Pump power absorbed by the SCF along the fiber length (colour online)

3. Improve absorbed power of SCF with FITC fluorescent material

To further improve the solar power absorbed by the SCF, the hollow reflector is filled with FITC fluorescent material [31-32]. The Nd:YAG SCF has five pump absorption bands for sunlight spectrum, which are 530 nm, 580 nm, 750 nm, 810 nm and 870 nm [33]. The interaction of sunlight and fluorescent material mainly includes three processes of sunlight absorption, excitation and fluorescence emission. The key criteria for selecting fluorescent sensitized materials include high fluorescence efficiency, and good spectral matching between the emission spectrum and Nd:YAG's absorption spectrum. The fluorescence efficiency of FITC material is 92%. The absorption and reflection spectra of FITC are shown in Fig. 3 [34-37]. The absorption spectrum of the FITC fluorescent material is from 455 nm to 512 nm, and the emission spectrum is located between 516 nm and 560 nm, which overlaps with the absorption band of the Nd-doped SCF (~530 nm).

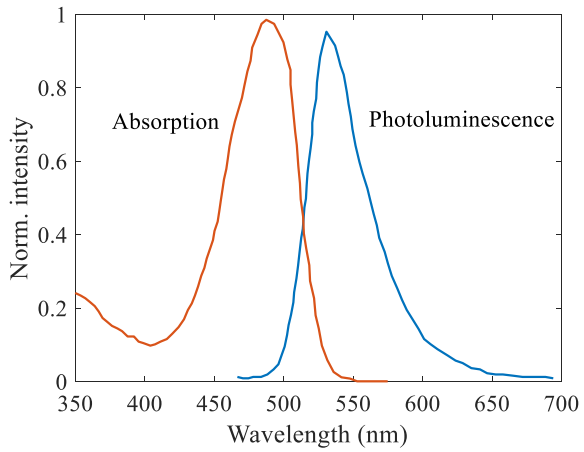

Fig. 3. Absorption and emission spectrum of FITC (colour online)

In single- and dual-end-pumped configurations, the Fig. 4 shows the percentage increase in the absorption pump power of SCF with fluorescent material in reflector, compared to non-sensitized systems. At a length of 40 mm, the absorbed pump power of SCF increases by 24.15% and 19.38% in single- and dual-end-pumped configuration, respectively. However, the improvement effect of FITC fluorescent material decreases with increasing fiber length. When the fiber length increases to 100 mm, the absorbed pump power of SCF increases by 21.29% and 17.31% in single- and dual-end-pumped configuration, respectively. The incorporation of FITC fluorescent material significantly improves in the single-end-pumped configuration compared to the dual-end-pumped systems.

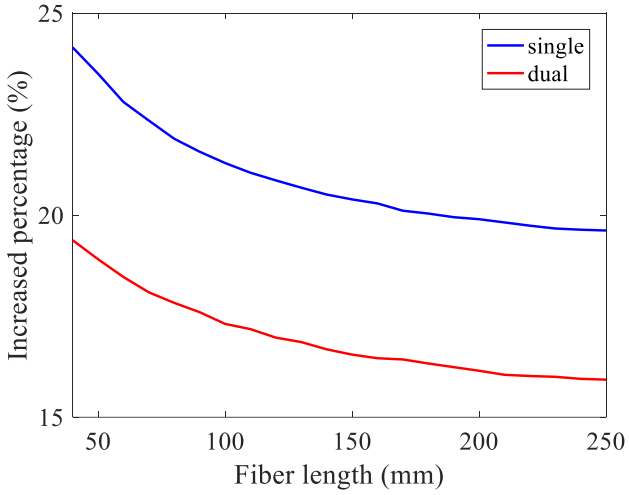

Fig. 4. Percent of power absorbed by SCF increases with fiber length (colour online)

As an example, a solar single-end-pumped SCF (Φ1 ×100 mm) is employed to calculate the laser output characteristics. When the distance of the fiber offset from the central axis varies from 0 mm to 2.2 mm, the optimal fiber positions for single- and dual-end-pumped configuration are 2 mm and 1.4 mm, respectively. Then, the comparison of SCF's absorption power in single- and dual-end-pumped configurations with or without FITC fluorescent material is shown in Fig. 5.

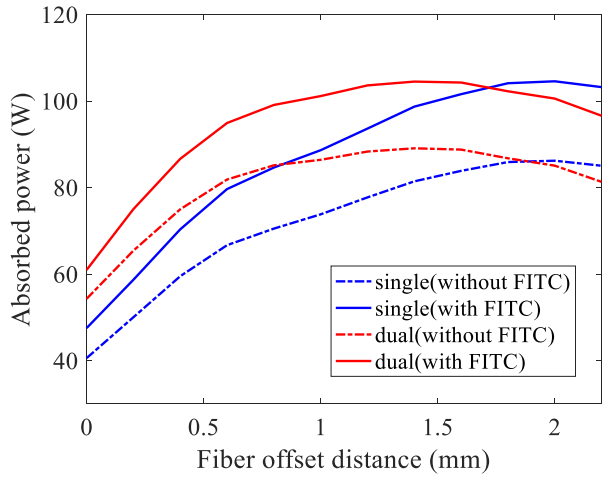

Fig. 5. Comparison of SCF's absorption power under single- and dual-end-pumped configuration (colour online)

In the single-end-pumped configuration, ray tracing based on Tracepro shows that the maximum absorbed power of SCF reaches 104.58 W at 2 mm offset from the central axis with FITC, which enhanced by 21.29% compared to 86.22 W of non-sensitized system. However, the maximum absorbed power of dual-end-pumped SCF is 104.51 W at 1.4 mm offset from the central axis with FITC, which increased by 17.31% compared to 89.09 W of non-sensitized systems.

4. Laser output characteristics

At steady state, rate equations and transmission equations of solar pumped Nd:YAG SCF are given as [38]:

$$\frac{dn_2(z,t)}{dt}=\frac{\frac{1}{An_0h}\sum_{k=1}^{K}\frac{\eta_Q(\lambda_k)P_P(z,\lambda_k)}{\nu_p(\lambda_k)}}{\frac{1}{An_0h}\sum_{k=1}^{K}\frac{\eta_Q(\lambda_k)P_P(z,\lambda_k)}{\nu_p(\lambda_k)}+\frac{1}{\tau_f}+\frac{\sigma_{es}P_s(z)}{Ah\nu_s}}-\frac{n_2(z,t)}{n_0},k=1,2,3...K \tag{1}$$

$$\frac{dp_s^{\pm}(z)}{dz}=\pm(\sigma_{es}n_2(z)-\alpha_s)P_s^{\pm}(z) \tag{2}$$

At steady state, the population densities in each energy level does not vary with time, then there is $dn_2(z,t)/dt=0$. Where n_2 is the upper-level populations, and η_Q is the quantum efficiency. P_P denotes the solar power absorbed per millimeter of the SCF based on ray tracing, and P_s is the signal optical power. K denotes the number of absorption bands of Nd:YAG SCF within the solar spectrum, and ν_p is the pump light frequency. Where $P_s^{\pm}(z)$ represent the signal power of forward (or backward) transmission in the SCF, respectively, and α_s denotes the loss of the signal light. Other relevant parameters are shown in Table 1.

Table 1. Parameters for simulation of solar pumped laser

Symbol	Parameter	Value
n_0	Population densities of the total Nd ions	1.38×10^{17}cm^{-3}
σ_{es}	Emission cross sections of the Nd:YAG SCF	3×10^{-17}cm^2
τ_f	Upper state lifetime	2.3×10^{-4}s
A	Cross-sectional area of the SCF	0.7854 mm^2
h	Planck's constant	6.626×10^{-34}
ν_s	Signal frequency	2.8195×10^{14}Hz

$P_s^+(0)=R_1P_s^-(0)$ and $P_s^-(L)=R_2P_s^+(L)$ are the boundary conditions for Equation (2). L is the length of the SCF, and $R_2(z=L)$ denotes the reflectivity of the output coupler. The reflectivity $R_1(z=0)$ of the other cavity mirror is set to 100%.

Taking a Nd:YAG SCF (Φ1 × 100 mm, 1 at.% doping concentration) as an example, the absorbed power per millimeter of solar single-ended pumped SCF with/without FITC sensitizing solution can be obtained (Fig. 6). The absorbed power per millimeter along the SCF decreases as the fiber length increases.

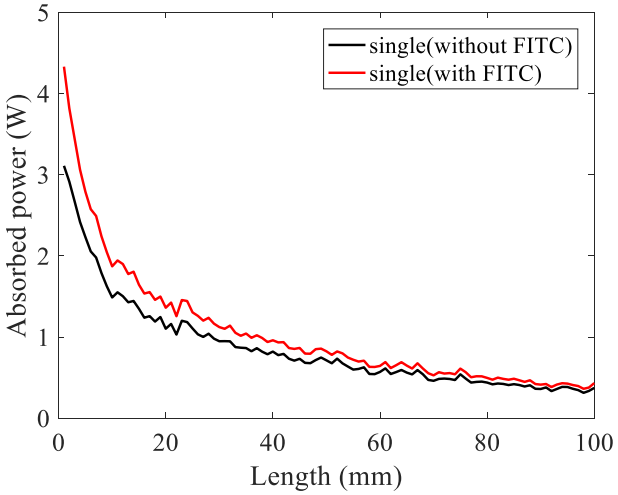

Fig. 6. Absorbed power of SCF with/without FITC in reflector (colour online)

Based on Comsol software, the temperature distribution of SCF with FITC fluorescent solution can be analyzed. The SCF is placed inside a hollow fused silica glass tube, where the cooling water temperature is

maintained at 20 °C. Based on MATLAB software, the temperature distribution along the axial direction of the SCF is shown in Fig. 7. The maximum temperature at the input end of the SCF is 85.92 °C, while the temperature drops to about 30 °C after a distance of 50 mm. The radial temperature distributions of the SCF at positions 1 mm, 50 mm and 100 mm are given in the inset in Fig. 7. The highest temperatures are all located at the axial position of the SCF, and are 85.92 °C, 32.22 °C and 26.29 °C, respectively. The lowest temperatures of 76.27 °C, 30.43 °C and 25.37 °C are all located at the surface of the SCF.

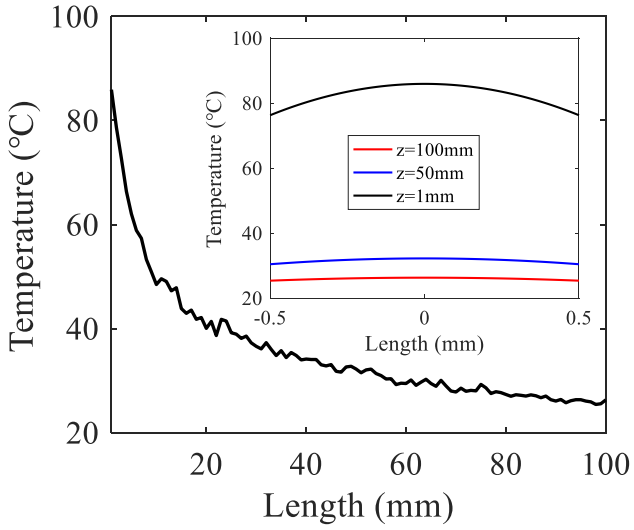

Fig. 7. A Temperature distribution of SCF at different locations in axial and radial directions (colour online)

Numerical analysis of the rate equations combined with optical transmission modeling reveals the dependence between the generated laser power and incoming solar power of single-end-pumped SCF laser with/without FITC, as presented in Fig. 8.

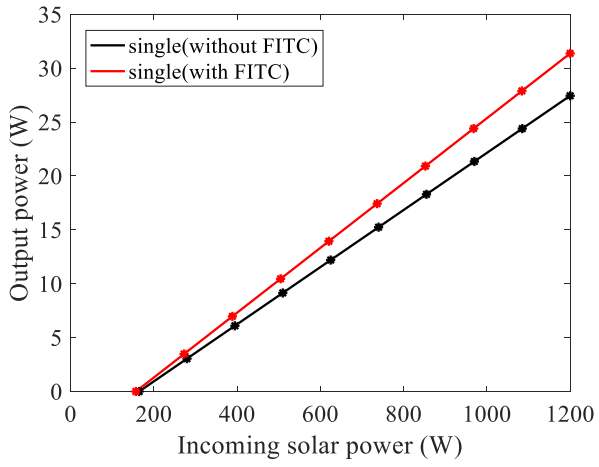

Fig. 8. Relationship between output power and incoming solar power for single-end-pumped configuration with/without FITC fluorescent solution (colour online)

Without sensitization solution, the pumping threshold, maximum output power, slope efficiency, and solar-to-laser conversion efficiency are 164.64 W, 27.45 W, 2.65% and 2.29%, respectively, when the SCF's absorption power and R_2 are 86.22 W and 68%. With the FITC fluorescence sensitizing solution in reflector, the pumping threshold, maximum output power, slope efficiency and solar-to-laser conversion efficiency are 156.91 W, 31.38 W, 3.01% and 2.62%, respectively, when the SCF's absorption power and R_2 are 104.58 W and 66%. With FITC fluorescent material in reflector, the absorbed power and the output power improve by 21.29% and 14.32%, respectively, compared to non-sensitized systems.

5. Conclusion

A approach to enhance the output power of solar-pumped SCF lasers by the reflector filled with fluorescence sensitizing solution is proposed. A three-stage concentrator comprises parabolic mirror/off-axis parabolic mirrors, 3D-CPC, and a hollow reflector housing the SCF. The influence of hollow reflector with/without the FITC fluorescence solution on the absorbed solar power of Nd:YAG SCF (Φ1×100 mm, 1 at.%) are compared between single- and dual-end-pumped configurations. Ray tracing with Tracepro shows that the absorbed power of the dual-end-pumped fiber reaches 104.51 W with a 17.31% improvement compared to non-sensitized systems. The SCF's maximum absorbed power in single-end-pumped configuration with FITC fluorescent solution is 104.58 W, which is 21.29% higher than that of non-sensitized systems. The simulations also demonstrate that the laser output power and the solar-to-laser conversion efficiency of the SCF in single-end-pumped configuration with FITC fluorescent solution are 31.38 W and 2.62 %, respectively. The laser output power is 14.32% higher than that of non-sensitized systems. This approach provides an idea to improve the output power or efficiency of solar-pumped SCF lasers.

Disclosures

The authors declare no conflicts of interest.

Acknowledgment

This work is supported by Research Fund of China Three Gorges University (SDHZ2022369).

References

[1] M. H. Ahmadi, M. Ghazvini, M. Sadeghzadeh, M. A. Nazari, R. Kumar, A. Naeimi, T. Ming,

Energy Sci. Eng. **6**(5), 340 (2018).
[2] J. Khan, M. H. Arsalan, Renewable Sustainable Energy Rev. **55**, 414 (2016).
[3] M. Küblböck, J. Will, H. Fattahi, APL Photonics **9**(5), 050903 (2024).
[4] T. Yabe, B. Bagheri, T. Ohkubo, S. Uchida, K. Yoshida, T. Funatsu, T. Oishi, K. Daito, M. Ishioka, N. Yasunaga, Y. Sato, C. Baasandash, Y. Okamoto, K. Yanagitani, J. Appl. Phys. **104**(8), 083104 (2008).
[5] D. Liang, J. Almeida, Opt. Express **21**(21), 25107 (2013).
[6] S. Mizuno, H. Ito, K. Hasegawa, T. Suzuki, Y. Ohishi, Opt. Express **20**(6), 5891 (2012).
[7] J. Zhu, Y. Liu, L. Lan, Y. Tang, Y. Zhang, X. Ma, Laser Phys. Lett. **20**(12), 125101(2023).
[8] B. Liu, P. R. Ohodnicki, Adv. Mater. Technol. **6**(9), 2100125 (2021).
[9] X. Délen, I. Martial, J. Didierjean, N. Aubry, D. Sangla, F. Balembois, P. Georges, Appl. Phys. B **104**(1), 1 (2011).
[10] X. Délen, S. Piehler, J. Didierjean, N. Aubry, A. Voss, M. A. Ahmed, T. Graf, F. Balembois, P. Georges, Opt. Lett. **37**(14), 2898 (2012).
[11] Z. R. Liu, K. Deng, M. Ma, J. Liu, Y. Liu, L. Lan, J. Zhou, Y. Lu, J. Russ. Laser Res. **45**(4), 435 (2024).
[12] B. Q. Wang, L. Lan, Y. Liu, Y. Tang, Y. Zhang, J. Russ. Laser Res. **44**(6), 682 (2023).
[13] W. T. Fan, Y. Liu, P. Guo, R. Deng, N. Li, F. Ding, Y. Li, J. Zhou, S. Xie, Curr. Opt. Photonics **4**(1), 50 (2020).
[14] R. M. Ribeiro, A. B. A. Fiasca, P. A. M. Dos Santos, R. Ribeiro, A. Fiasca, P. A. Santos, M. Andreeta, A. Hernandes, Opt. Mater. **10**(3), 201 (1998).
[15] W. Que, Y. Zhou, Y. L. Lam, Y. C. Chan, C. H. Kam, Y. Huo, L. Zhang, X. Yao, J. Mod. Opt. **47**(6). 1127 (2000).
[16] R. K. Nubling, J. A. Harrington, Appl. Opt. **36**(24), 5934 (1997).
[17] L. H. Ye, Rev. Sci. Instrum. **77**(5), 054901 (2006)
[18] J. A. Harrington, Proc. SPIE **8959**, 895902 (2014).
[19] K. Zheng, Y. Liu, L. Lan, Y. Zhang, Opt. Fiber Technol. **95**, 104390 (2025).
[20] H. Costa, D. Liang, J. Almeida, M. Catela, D. Garcia, B. D. Tibúrcio, C. R. Vistas, Energies **15**(23), 9140 (2022).
[21] D. Liang, J. Almeida, D. Garcia, B. D. Tibúrcio, E. Guillot, C. R. Vistas, Sol. Energy **199**, 192 (2020).
[22] J. Almeida, D. Liang, M. Catela, H. Costa, D. Garcia, B. D. Tibúrcio, E. Guillot, C. Vistas, Opt. Express **31**(24), 40041 (2023).
[23] B. Villars, E. S. Hill, C. G. Durfee, Opt. Lett. **40**(13), 3049 (2015).
[24] T. Masuda, M. Iyoda, Y. Yasumatsu, M. Endo, Opt. Lett. **42**(17), 3427 (2017).
[25] M. Endo, J. F. Bisson, T. Masuda, Jpn. J. Appl. Phys. **58**(11), 112006 (2019).
[26] T. Masuda, M. Iyoda, Y. Yasumatsu, S. Dottermusch, I. A. Howard, B. S. Richards, J. Bisson, M. Endo, Commun. Phys. **3**(1), 60 (2020).
[27] T. Masuda, Y. Zhang, C. Ding, F. Liu, K. Sasaki, Q. Shen, M. Endo, J. Appl. Phys. **127**(24), 243104 (2020).
[28] A. G. Kakhkhorov, A. A. Sherniyozov, S. D. Payziyev, Uzb. J. Phys. **23**(2), 71 (2023).
[29] W. Koechner, Solid-State Laser Engineering, Springer, New York, America **48**, 2005.
[30] C. R. Vistas, D. Liang, J. Almeida, Sol. Energy **122**, 1325 (2015).
[31] J. R. Lakowicz, Principles of Fluorescence Spectroscopy, Boston, MA: Springer US, 1-23 (1999).
[32] C. E. Wheelock, J. Am. Chem. Soc. **81**(6), 1348 (1959).
[33] J. Zhang, C. Zhao, Z. Cai, Z. Zhao, Chin. J. Lasers **50**(13), 1301002 (2023).
[34] T. T. Nguyen, H. N. Nguyen, T. H. L. Nghiem, X. H. Do, T. T. To, T. X. P. Do, D. L. Do, H. G. Nguyen, H. M. Nguyen, N. D. Nguyen, M. Q. Luu, T. N. Nguyen, T. B. N. Nguyen, V. T. Nguyen, V. T. Pham, U. T. T. Than, T. M. N. Hoang, Sci. Rep. **14**(1), 6969 (2024).
[35] A. Imhof, M. Megens, J. J. Engelberts, D. T. N. D. Lang, R. Sprik, W. L. Vos, J. Phys. Chem. B **103**(9), 1408 (1999).
[36] B. S. Kim, J. M. Oh, K. S. Kim, K. S. Seo, J. S. Cho, G. Khang, H. B. Lee, K. Park, M. S. Kim, Biomaterials **30**(5), 902 (2009).
[37] A. Hoffmann, J. Bredno, M. Wendland, N. Derugin, P. Ohara, M. Wintermark, Transl. Stroke Res. **2**(1), 106 (2011).
[38] I. H. Hwang, J. H. Lee, IEEE J. Quantum Electron. **27**(9), 2129 (1991).

*Corresponding author: liuyan703@163.com
240014775@qq.com